




High infrared transparency up to 8- μ m-wavelength in correlated vanadium Wadsley conductors

Cite as: APL Mater. 8, 041111 (2020); <https://doi.org/10.1063/1.5136059>

Submitted: 11 November 2019 . Accepted: 22 March 2020 . Published Online: 14 April 2020

Songhee Choi, Joongoo Kang , Sangkyun Ryu, Hyungjeen Jeon , Jaeseok Son, and Shinbuhm Lee 



View Online



Export Citation



CrossMark

ARTICLES YOU MAY BE INTERESTED IN

[New approaches for achieving more perfect transition metal oxide thin films](#)

APL Materials **8**, 040904 (2020); <https://doi.org/10.1063/5.0003268>

[Emergent behavior of LaNiO₃ in short-periodic nickelate superlattices](#)

APL Materials **8**, 041113 (2020); <https://doi.org/10.1063/5.0004530>

[Aspects of the synthesis of thin film superconducting infinite-layer nickelates](#)

APL Materials **8**, 041107 (2020); <https://doi.org/10.1063/5.0005103>

APL Materials

SPECIAL TOPIC: Open Framework Materials for Energy Applications

Now Online!

High infrared transparency up to 8- μm -wavelength in correlated vanadium Wadsley conductors

Cite as: APL Mater. 8, 041111 (2020); doi: 10.1063/1.5136059

Submitted: 11 November 2019 • Accepted: 22 March 2020 •

Published Online: 14 April 2020



Songhee Choi,¹ Joongoo Kang,¹  Sangkyun Ryu,² Hyungjeen Jeon,²  Jaeseok Son,³ and Shinbuhm Lee^{1,a)} 

AFFILIATIONS

¹Department of Emerging Materials Science, Daegu-Gyeongbuk Institute of Science and Technology, Daegu 42988, South Korea

²Department of Physics, Pusan National University, Busan 46241, South Korea

³Center for Correlated Electron Systems, Institute for Basic Science and Department of Physics and Astronomy, Seoul National University, Seoul 08826, South Korea

^{a)} Author to whom correspondence should be addressed: lee.shinbuhm@dgist.ac.kr

ABSTRACT

Within industrial and military contexts, research on infrared transparent conductors (IR-TCs) has been limited due to the significant suppression of transparency by the free electron response. In this paper, we report that strong correlations between electrons play an important role in the development of a new strategy for fabricating IR-TCs. Metallic $\text{VO}_2(\text{B})$ and V_6O_{13} persistently exhibit transmittances 45% higher than that of Sn-doped In_2O_3 for a broad IR wavelength range of up to 8 μm . Based on electronic band structures determined quantitatively using x-ray absorption spectroscopy, x-ray photoemission spectroscopy, and spectroscopic ellipsometry, we propose that the enhancement in the IR-TC is attributed to the redshift of the plasma frequency induced by the correlated electrons.

© 2020 Author(s). All article content, except where otherwise noted, is licensed under a Creative Commons Attribution (CC BY) license (<http://creativecommons.org/licenses/by/4.0/>). <https://doi.org/10.1063/1.5136059>

Infrared transparent conductors (IR-TCs) have attracted considerable attention for a range of possible applications, including smart windows, transparent solar cells, IR sensors, and protective window coatings for guided weapons and IR searchers of aircraft.¹ To date, the development of TCs (e.g., metals and doped semiconductors) has focused on high transmittance, mainly in the visible range,^{2–8} so we still lack the technology and processes to create IR-TCs. Most conductors are intrinsically opaque at IR wavelengths, and low resistivity and high IR transparency are mutually exclusive. In metals and doped semiconductors, free electron oscillations induced by electromagnetic waves suggest the existence of a plasma frequency.⁹ At frequencies below the plasma frequency, free electrons reflect light. As doped semiconductors contain fewer electrons than metals, plasma edges occur at frequencies in the visible range for metals and in the near-IR range for doped semiconductors. Thus, the realization of IR-TCs is intrinsically challenging when using conventional TCs.

Despite the challenges, there have been a few trials aimed at developing IR-TCs. The simplest way to improve the IR transmittance is to reduce the thickness of the device. When light is propagating through a material, the intensity measured at the opposite side increases exponentially with a decrease in the thickness, and the phenomenon is known as Beer's law.⁹ Although high transparency is achieved in ultrathin films, the sheet resistance increases abruptly because the film thickness is smaller than the electron scattering length. To overcome this trade-off, conventional TCs with high carrier mobility, μ , have attracted attention. According to the free electron model, high μ assists conventional TCs in retaining considerable conductivity, $\sigma (=eN\mu)$, where e is the electric charge and N is the carrier density, even with low N and without significant loss of conductivity; thus, the plasma frequency can shift to the far-IR range as it is proportional to \sqrt{N} . The IR transmittance of In_2O_3 doped with either transition metals or hydrogen ($\mu \sim 130 \text{ cm}^2 \text{ V}^{-1} \text{ s}^{-1}$) is slightly improved.^{10–12} However, this approach generally leads to

extremely poor crystallinity due to “doping bottlenecks.” Various materials, such as carbon-based nanomaterials,¹³ have been studied as potential IR-TC candidates. However, currently used materials do not perform optimally, and new approaches to developing IR-TCs are highly necessary.

Herein, we propose a new type of intrinsic IR-TC based on strong correlations between electrons (SCEs) in transition metal oxides. Transmittance persistently exceeded 70% in the IR wavelength range up to 8 μm in metallic $\text{VO}_2(\text{B})$ and V_6O_{13} . To understand the simultaneous attainment of IR transparency and metallic requirements, we quantitatively investigated the electronic band structures of these materials using x-ray absorption spectroscopy (XAS), x-ray photoemission spectrometry (XPS), and using a spectroscopic ellipsometer (SE). We found that SCEs play an important role in creating IR-TCs.

Next-generation IR-TCs should exhibit two important features: (i) high and persistent transmittance at IR wavelengths and (ii) low resistivity. Figure 1(a) schematically shows the desired transmittance features of IR-TCs, as well as the general behavior of insulators and conventional TCs. Suppression of transmittance is commonly observed at ultraviolet wavelengths in all materials due to interband transitions, in which electrons transition from occupied to unoccupied bands. The insulator and conventional TC are transparent and opaque to IR, respectively, because the latter exhibits free electron response. Therefore, for an IR-TC, we aim to obtain high levels of transmittance at IR wavelengths, with levels close to those of insulators.

Metallic $\text{VO}_2(\text{B})$ and V_6O_{13} exhibit a high transmittance of greater than 90% at wavelengths of 8 μm , as shown in Fig. 1(b). The insulating nature of V_2O_5 prohibits it from being used in IR-TC applications although V_2O_5 exhibits almost 100% transmittance over IR wavelengths (not shown here). For comparison, as shown in the schematic of Fig. 1(a), we also included the transmittance data from conventional TC Sn-doped In_2O_3 (ITO). While ITO exhibits high transmittance, almost 90% at visible wavelengths, the transmittance decreases gradually with an

increase in the wavelength, i.e., 45% at a wavelength of 8 μm . Our $\text{VO}_2(\text{B})$ and V_6O_{13} films exhibit a transmittance of 45% higher than that of ITO at a wavelength of 8 μm . The transmittance sharply decreased and increased below 400-nm wavelength and above 8- μm wavelength, respectively, due to interband transition and antireflection effects, defining the fundamental absorption edge of $\text{VO}_2(\text{B})$ and V_6O_{13} . As shown in Fig. 1(c), $\text{VO}_2(\text{B})$ and V_6O_{13} exhibit low resistivities of 8.3 m Ω cm and 3.9 m Ω cm at room temperature, respectively, comparable to those of conventional TCs, such as ITO, In_2O_3 , and La-doped BaSnO_3 . It is somewhat surprising that $\text{VO}_2(\text{B})$ and V_6O_{13} fulfill two critical requirements, namely, high IR transmittance and low resistivity, which have not been previously observed simultaneously in metals and doped semiconductors. The experimental deposition method, structural properties, and electrical properties of the samples in this work are detailed in Secs. 1–3 of the [supplementary material](#), respectively.

The electronic band structure is widely used to understand the unique interplay between the transparency and the resistivity in TCs.^{3–8} Therefore, it is worth investigating the electronic band structures of $\text{VO}_2(\text{B})$ and V_6O_{13} to understand their IR-TC characteristics. Note that $\text{VO}_2(\text{B})$, V_6O_{13} , and V_2O_5 belong to the vanadium Wadsley series, $\text{V}_m\text{O}_{2m+1}$ ($m > 1$, integer).¹⁴ The end members of the Wadsley phases are V_2O_5 ($m = 2$) and VO_2 ($m = \infty$), with single oxidation states of V^{5+} and V^{4+} , respectively. V_3O_7 ($m = 3$) and V_6O_{13} ($m = 6$) have mixed oxidation states between V^{5+} and V^{4+} . Therefore, the vanadium Wadsley series represents a prototypical model to establish electronic band structures in terms of systematic changes in the number of electrons in the outermost 3d orbital, e.g., d^1 in $\text{VO}_2(\text{B})$, d^x ($0 < x < 1$) in V_6O_{13} and V_3O_7 , and d^0 in V_2O_5 . We used XAS, XPS, and SE to quantitatively establish the electronic band structure and understand the unusually high IR transmittance in metallic $\text{VO}_2(\text{B})$ and V_6O_{13} .

We carried out XAS at room temperature to investigate the conduction bands of $\text{VO}_2(\text{B})$ and V_6O_{13} . For comparison, we also performed the same measurement for V_2O_5 . Figure 2(a) shows the V- L_3 and V- L_2 edge spectra located in the range of 512–526 eV.

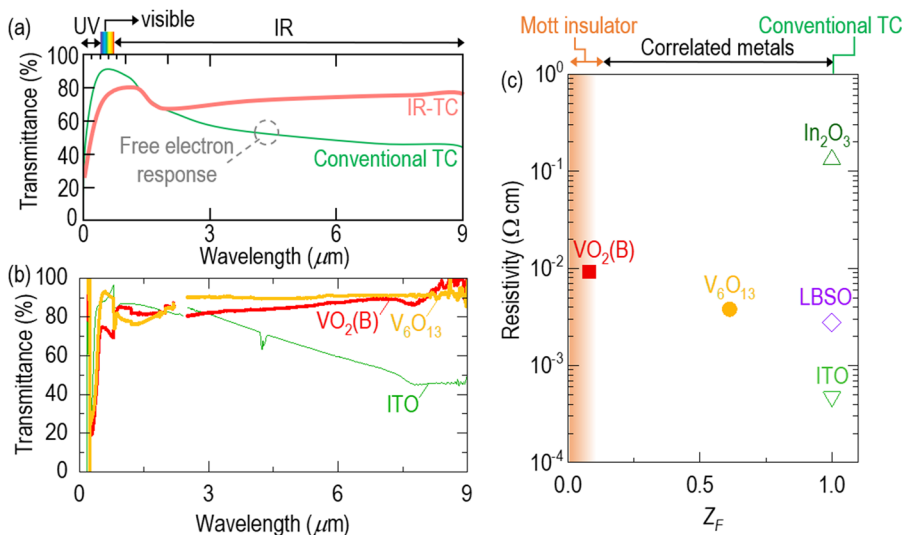


FIG. 1. (a) Prototypical transmittance behavior for an IR-TC and conventional TC. While the transmittance of conventional TCs is typically suppressed at far-IR wavelengths due to the free electron response, IR-TCs should exhibit high and persistent transmittance in this range. (b) High (>70%) and persistent transmittance of metallic $\text{VO}_2(\text{B})$ and V_6O_{13} in a wide IR range up to 8 μm . Comparatively, the transparent conducting Sn-doped In_2O_3 exhibits suppressed transmittance in the far-IR region. (c) Distribution of resistivity and electron correlation strength Z_F . The resistivities of correlated metals, $\text{VO}_2(\text{B})$ ($Z_F = 0.08$) and V_6O_{13} ($Z_F = 0.61$), are comparable to those of conventional TCs ($Z_F = 1$). ITO and LBSO denote Sn-doped In_2O_3 and La-doped BaSnO_3 , respectively.

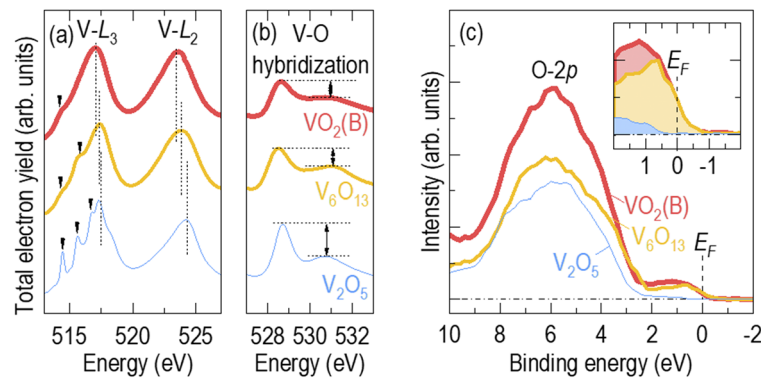


FIG. 2. Spectroscopic measurements to quantitatively establish the electronic band structures of $\text{VO}_2(\text{B})$, V_6O_{13} , and V_2O_5 . We analyzed x-ray absorption total electron yield spectra to investigate the conduction bands of $\text{VO}_2(\text{B})$, V_6O_{13} , and V_2O_5 . (a) V- L_3 and V- L_2 spectra in the range 512–526 eV. As indicated by the small arrows, there are two, three, and four peaks in the V- L_3 spectra of $\text{VO}_2(\text{B})$, V_6O_{13} , and V_2O_5 , respectively. The vertical dashed lines emphasize the shifts in the V- L_3 and V- L_2 peaks, which indicate variation in V oxidation states. (b) Spectra originating from hybridization of O-2p and V-3d orbitals in the range 527–533 eV. The longer double-headed arrows represent larger intensity differences between the first and second peaks, indicating larger populations of electrons in t_{2g} bands and weaker hybridization between O-2p and V-3d orbitals. (c) X-ray photoemission spectroscopy near the Fermi energy (E_F) was used to investigate the valence bands of $\text{VO}_2(\text{B})$, V_6O_{13} , and V_2O_5 . $\text{VO}_2(\text{B})$ and V_6O_{13} exhibit a significant spectral weight (enlarged in the inset) near E_F , while V_2O_5 does not. This peak indicates the existence of occupied bands, primarily dominated by electrons in V-3d orbitals. The O-2p orbital makes the main contribution to the large spectral weight centered at 6 eV.

The former and latter spectra appear due to the transition from V- L_3 and V- L_2 core levels to unoccupied 3d conduction bands. The spectra are similar to the XAS reports in the literature.^{15,16} As indicated by the small arrows, the V- L_3 spectra exhibit two [$\text{VO}_2(\text{B})$], three (V_6O_{13}), and four (V_2O_5) peaks with an increase in the oxygen content. Multiple transitions are allowed using the x-ray absorption process, as exemplified by V_2O_5 ,^{17,18} due to the symmetry and metal–oxygen hybridization. Furthermore, as the number of outermost electrons decreases from $3d^1$ [$\text{VO}_2(\text{B})$] to $3d^0$ (V_2O_5), the V- L_3 and V- L_2 peaks shift toward higher energies, as highlighted by the dotted lines. This shift represents the increasing oxidation states of vanadium ions ($\text{V}^{4+} \rightarrow \text{V}^{5+}$), which are consistent with XPS observations.^{14,16,19,20} Figure 2(b) shows XAS spectra representing the hybridization of O-2p and V-3d orbitals in the range of 527–533 eV. The difference in the intensity marked by the double-headed arrows decreases with an increase in the number of electrons in the V-3d orbitals, indicating higher electron populations in t_{2g} bands and weaker hybridization.

To obtain information regarding the valence band of IR-TCs composed of $\text{VO}_2(\text{B})$ and V_6O_{13} , we carried out XPS near the Fermi energy, with binding energies in the range of –2 eV to 10 eV. As shown in Fig. 2(c), there is a large spectral weight near 2–10 eV, which is mainly attributed to the O-2p orbital.¹⁶ At –1 eV to 2 eV, around the Fermi energy (dashed line), we observed a considerable spectral weight for $\text{VO}_2(\text{B})$ and V_6O_{13} , which is more clearly shown in the inset. This indicates the existence of valence bands over the Fermi energy, consistent with the metallic properties of $\text{VO}_2(\text{B})$ and V_6O_{13} . In contrast, there is a negligible spectral weight for V_2O_5 near the Fermi energy, which is also consistent with the insulating properties of V_2O_5 at room temperature.

Although the XPS and XAS results together demonstrate the metallic electronic band structures of $\text{VO}_2(\text{B})$ and V_6O_{13} , it is interesting to note that $\text{VO}_2(\text{B})$ and V_6O_{13} exhibit high IR transmittance, which is not achieved using typical metals and doped

semiconductors. To better understand this unexpected discrepancy, we measured the optical conductivity using SE, which can provide information on the joint density of states. Figure 3 shows the optical conductivity of $\text{VO}_2(\text{B})$, V_6O_{13} , and V_2O_5 in the photon range of 0.01–6 eV. The peak near 1 eV, observed only in $\text{VO}_2(\text{B})$ and V_6O_{13} , was expected due to the optical transition from occupied t_{2g} to unoccupied t_{2g} bands. The peaks above 3 eV are attributed to interband transitions from O-2p to unoccupied t_{2g} bands and from occupied t_{2g} to unoccupied e_g bands. By performing density functional theory (DFT) calculations with the assumption of the presence of free electrons, we successfully reproduced the general features of the interband transitions of $\text{VO}_2(\text{B})$, V_6O_{13} , and V_2O_5 , as indicated by the dashed lines in Figs. 3(d)–3(f). However, it should be noted that, in contrast, with an increase in the Drude spectra near 0 eV in DFT (comb-patterns) due to the free electron response, the experimental spectra for metallic $\text{VO}_2(\text{B})$ and V_6O_{13} were suppressed, showing a convex form. To understand this unconventional behavior in more detail, we resolved the experimentally measured optical conductivity using the Drude–Lorentz model, $\sigma_1(\omega) = \frac{e^2}{m^*} \frac{N_D \gamma_D}{\omega^2 + \gamma_D^2} + \frac{e^2}{m^*} \sum_j \frac{N_j \gamma_j \omega^2}{(\omega_j^2 - \omega^2)^2 + \gamma_j^2 \omega^2}$, where m^* , γ_j , and ω_j are the effective mass, damping coefficient, and angular frequency of the j th resonance line, respectively.⁹ The first and second terms represent the Drude model of free electron conductivity and the Lorentz model of dipole oscillators for interband transitions, respectively. We could fit the optical conductivity perfectly using several Lorentz oscillators (lightly shaded lines). The experimental Drude responses [comb-patterns in Figs. 3(a) and 3(b)] were significantly suppressed compared with those obtained from DFT [comb-patterns in Figs. 3(d) and 3(e) calculated with the assumption $\hbar\gamma_D = 0.1$ eV of typical metals²¹]. Interestingly, the Drude response in $\text{VO}_2(\text{B})$ is experimentally more suppressed than that in V_6O_{13} , while according to DFT, $\text{VO}_2(\text{B})$ exhibits a more pronounced Drude response than V_6O_{13} due to the extra electrons in $\text{VO}_2(\text{B})$. Therefore, we hypothesize that another mechanism, beyond the simple free electron

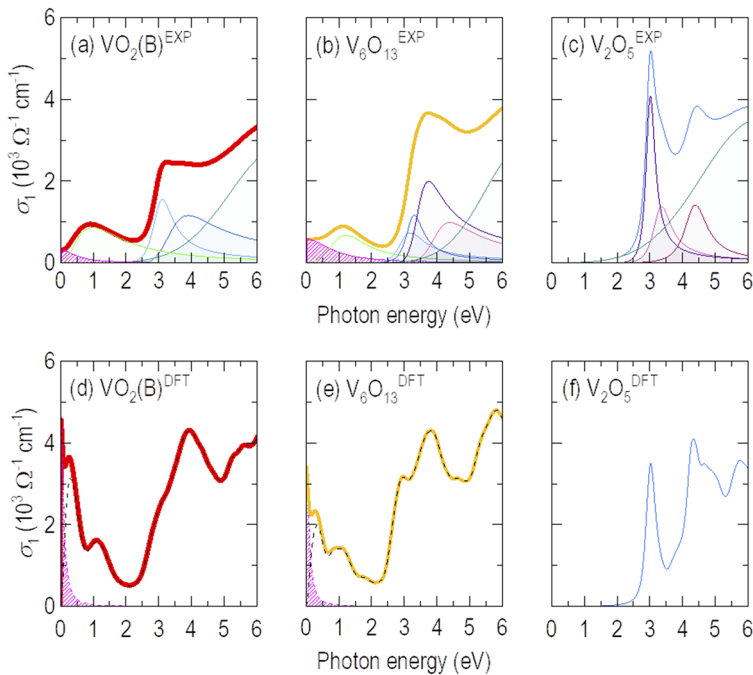


FIG. 3. Optical conductivity of (a) VO₂(B), (b) V₆O₁₃, and (c) V₂O₅. Due to electron correlation, the spectral intensity near 0 eV becomes suppressed, showing a convex form in metallic VO₂(B) and V₆O₁₃. There is negligible intensity in the case of insulating V₂O₅. We fitted the spectra using the Drude–Lorentz model, which represents the Drude response (comb-pattern) and Lorentz oscillators of interband transitions (lightly shaded lines). For comparison, we calculated the optical conductivity of (d) VO₂(B), (e) V₆O₁₃, and (f) V₂O₅ by density functional theory (DFT), without any influence of electron correlation. The solid line represents the optical conductivity summed from the Drude response (comb-pattern) and interband transition (dashed line). The calculated optical conductivities of VO₂(B) and V₆O₁₃ indicate pronounced spectral intensity near 0 eV, in contrast to the experimentally measured values. The superscripts “EXP” and “DFT” stand for experimental data measured by spectroscopic ellipsometry and theoretical data calculated by the DFT, respectively.

model, plays an important role in the IR transparency of VO₂(B) and V₆O₁₃.

In comparison to conventional metals, electrons in correlated materials have a weaker Drude response.^{22–24} Vanadate is a well-known oxide that exhibits a variety of emergent properties due to SCEs in V-3d orbitals.^{25–33} The correlation-driven insulator VO₂(M1) (monoclinic, $a = 5.74$ Å, $b = 4.52$ Å, $c = 5.38$ Å, and $\beta = 122.6^\circ$) has a small band gap of ~ 0.6 eV at temperatures below 340 K and accordingly exhibits high IR transmittance.^{28,32,33} Comparatively, the transmittance of metallic VO₂(R) (tetragonal, $a = b = 4.55$ Å, and $c = 2.86$ Å) above 340 K is highly suppressed in the IR region due to the free electron response.²⁸ Likewise the high transmittance and metallicity of VO₂(B) and V₆O₁₃ may be due to their being in the vicinity of the Mott transition, between metals and insulators. Correlation effects reduce the optical absorption of free electrons, extending the transparent window to the IR region, with persistent metal-like transport.

The intermediate correlations of electrons are at the heart of our design strategy for developing IR-TCs. We employed the extended Drude formalism to understand the deviation from the conventional Drude theory.^{23,24} We quantified the electron correlation strength (in other words, the quasiparticle renormalization amplitude), $Z_F = (\omega_p^{\text{EXP}}/\omega_p^{\text{DFT}})^2$, by considering the plasma frequencies from experimentally determined ω_p^{EXP} for correlated electrons and DFT-calculated ω_p^{DFT} for non-interacting free electrons.^{23,24} We determined the plasma frequencies, $\omega_p^2 = 8 \int \sigma_1(\omega) d\omega$, from the Drude spectra (comb-patterns) of optical conductivity, as shown in Fig. 3.^{23,24} The plasma frequencies are $\hbar\omega_p^{\text{EXP}} = 0.51$ eV [VO₂(B)], 1.26 eV (V₆O₁₃), $\hbar\omega_p^{\text{DFT}} = 1.86$ eV [VO₂(B)], and 1.61 eV (V₆O₁₃). Therefore, the Z_F -values are 0.08 for VO₂(B) and 0.61 for V₆O₁₃, which are much reduced compared with those of conventional TCs

($Z_F = 1$) and comparable to that of the correlated metal SrVO₃ ($Z_F = 0.33 \pm 0.03$ with $\hbar\omega_p^{\text{EXP}} = 2.10$ eV and $\hbar\omega_p^{\text{DFT}} = 3.66$ eV).²⁴ In Fig. 1(c), we revised the room temperature resistivity of VO₂(B) and V₆O₁₃ as a function of Z_F . As the smaller Z_F in VO₂(B) reveals pronounced correlation effects, which finally diverge in Mott insulators, the resistivity of VO₂(B) is slightly higher than that of V₆O₁₃. By $Z_F (=m_b/m^*$, where m_b is the band mass and m^* is the effective mass),^{23,24} moreover, we could deduce that the effective masses of VO₂(B) and V₆O₁₃ are $m_b/0.08$ and $m_b/0.61$, respectively, which are larger than m_b due to strong correlation effects between electrons.

Figure 4 shows the proposed electronic band structures of VO₂(B), V₆O₁₃, and V₂O₅, which we quantified based on XAS, XPS, and SE measurements. The colored (uncolored) bands below (above) the Fermi energy indicate occupied (unoccupied) states. The t_{2g} and e_g bands are split by crystal fields, arising from strong V-3d and O-2p hybridization. As shown in Figs. 4(a) and 4(b), the t_{2g} bands are close below the Fermi energy for VO₂(B) and V₆O₁₃, indicating metallic properties. In contrast, as shown in Fig. 4(c), there are no bands at the Fermi energy of V₂O₅, representing the insulating behavior. The most important feature is that the energy gap of VO₂(B) and V₆O₁₃ is slightly open near the Fermi energy due to electron correlation effects. This gap is large enough to enhance IR transparency but small enough to allow low resistivity. Therefore, VO₂(B) and V₆O₁₃ are suitable for use as IR-TCs. There are more electrons in the V-3d orbitals of VO₂(B) than in V₆O₁₃, resulting in stronger correlations, so the gap opens slightly further, driving slightly higher resistivity [Fig. 1(c)]. Regardless of the gap between occupied and unoccupied t_{2g} bands, both VO₂(B) and V₆O₁₃ are metallic because these gaps are narrow (< 25 meV) enough to be overcome by thermal energy at room temperature.

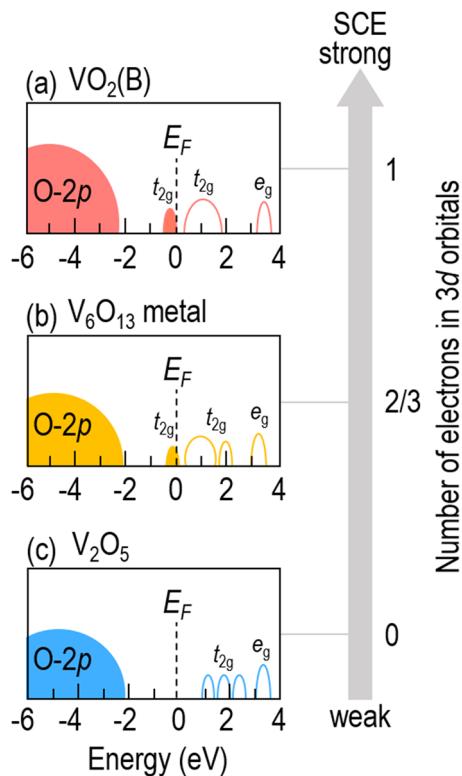


FIG. 4. Electrical band structures of (a) $\text{VO}_2(\text{B})$, (b) V_6O_{13} , and (c) V_2O_5 . We established these band structures quantitatively based on the results of our experiments, i.e., x-ray absorption spectroscopy [Figs. 2(a) and 2(b)], x-ray photoemission spectroscopy [Fig. 2(c)], and spectroscopic ellipsometry (Fig. 3). The colored half-circles below E_F indicate occupied O-2p and t_{2g} bands, and the uncolored half-circles indicate empty t_{2g} and e_g bands. There is a small gap (<25 meV) between occupied and unoccupied t_{2g} bands for $\text{VO}_2(\text{B})$ and V_6O_{13} . Since $\text{VO}_2(\text{B})$ ($m = \infty$), V_6O_{13} ($m = 6$), and V_2O_5 ($m = 2$) are in the series of vanadium Wadsley phases $\text{V}_m\text{O}_{2m+1}$ ($m > 1$, integer), the number of electrons in 3d orbitals increases systematically with an increase in m . The strong correlations between electrons (SCEs) will increase accordingly.

In conclusion, we introduced IR transparent conducting oxides utilizing SCEs. The vanadium oxides, $\text{VO}_2(\text{B})$ and V_6O_{13} , both exhibit not only low resistivities of 8.3 m Ω cm and 3.9 m Ω cm at room temperature, respectively, but also a persistent transparency exceeding 70% for wavelengths of up to 8 μm . Due to their superiority compared with conventional TCs, correlated oxides could potentially be used as IR-TCs. The electron correlation-based design strategy for IR-TCs is very promising as it overcomes the current limitations of transparent conductors, as mentioned in the Introduction. We achieved high IR transparency at room temperature and ambient pressure without cation doping. Rather than changing the carrier density, which is applied intensively in doped semiconductors, we used correlation effects to optimize the plasma frequency and resistivity simultaneously. $\text{VO}_2(\text{B})$ and V_6O_{13} are binary oxides that are more compatible with mass production than ternary oxides. Controlling correlations based on strain and field

effects, as well as smaller thicknesses, will improve the performance of IR-TCs.

See the [supplementary material](#) for the experimental method, x-ray diffraction θ - 2θ scans, x-ray reflectivity, and temperature dependence of resistivity.

AUTHOR'S CONTRIBUTIONS

S.C. conceived and designed the experiments under the supervision of S.L. S.C. fabricated the $\text{VO}_2(\text{B})$, V_6O_{13} , and V_2O_5 films. S.C. investigated the optical, structural, and electrical properties of the films. J.K. conducted DFT calculations. Under the guidance of S.L., S.C., and J.S. conducted SE at the Center for Correlated Electron System, Institute for Basic Science Center. Under the supervision of S.L. and H.J., S.C. and S.R. carried out XAS measurements at PLS-II. S.C. and S.L. wrote the manuscript, and the other authors reviewed it.

This work was supported by the Defense Acquisition Program Administration and Agency for Defense Development of Korea (Project No. 911223001). J.K. was supported by the National Research Foundation (NRF) of Korea (Project No. 2016R1C1B2016046). H.J. and S.R. were supported by the NRF (Project No. 2018M2A2B3A01071859). The work at PLS-II was supported in part by MSICT and POSTECH.

REFERENCES

- C. J. Traverse, R. Pandey, M. C. Barr, and R. R. Lunt, *Nat. Energy* **2**, 849 (2017).
- H. Kawazoe, M. Yasukawa, H. Hyodo, M. Kurita, H. Yanagi, and H. Hosono, *Nature* **389**, 939 (1997).
- H. Mizoguchi, T. Kamiya, S. Matsuishi, and H. Hosono, *Nat. Commun.* **2**, 470 (2011).
- H. J. Kim, U. Kim, T. H. Kim, J. Kim, H. M. Kim, B.-G. Jeon, W.-J. Lee, H. S. Mun, K. T. Hong, J. Yu, K. Char, and K. H. Kim, *Phys. Rev. B* **86**, 165205 (2012).
- X. Zhang, L. Zhang, J. D. Perkins, and A. Zunger, *Phys. Rev. Lett.* **115**, 176602 (2015).
- X. Yu, T. J. Marks, and A. Facchetti, *Nat. Mater.* **15**, 383 (2016).
- M. Morales-Masis, S. De Wolf, R. Woods-Robinson, J. W. Ager, and C. Ballif, *Adv. Electron. Mater.* **3**, 1600529 (2017).
- H. Hiramatsu, H. Yusa, R. Igarashi, Y. Ohishi, T. Kamiya, and H. Hosono, *Inorg. Chem.* **56**, 10535 (2017).
- M. Fox, *Optical Properties of Solids* (Oxford University Press, Oxford, United Kingdom, 2010).
- T. Koida, H. Fujiwara, and M. Kondo, *Jpn. J. Appl. Phys., Part 2* **46**, L685 (2007).
- B. Macco, H. C. M. Knoops, and W. M. M. Kessels, *ACS Appl. Mater. Interfaces* **7**, 16723 (2015).
- J. Xu, J.-B. Liu, B.-X. Liu, S.-N. Li, S.-H. Wei, and B. Huang, *Adv. Electron. Mater.* **4**, 1700553 (2018).
- L. Hu, D. S. Hecht, and G. Grüner, *Appl. Phys. Lett.* **94**, 081103 (2009).
- S. Choi, J. Son, J. Oh, J.-H. Lee, J. H. Jang, and S. Lee, *Phys. Rev. Mater.* **3**, 063401 (2019).
- M. Abbate, H. Pen, M. T. Czyżyk, F. M. F. de Groot, J. C. Fuggle, Y. J. Ma, C. T. Chen, F. Sette, A. Fujimori, Y. Ueda, and K. Kosuge, *J. Electron Spectrosc. Relat. Phenom.* **62**, 185 (1993).
- R. Zimmermann, R. Claessen, F. Reinert, P. Steiner, and S. Hüfner, *J. Phys.: Condens. Matter* **10**, 5697 (1998).
- A. Chakrabarti, K. Hermann, R. Druzinic, M. Witko, F. Wagner, and M. Petersen, *Phys. Rev. B* **59**, 10583 (1999).
- R. J. O. Mossane, A. Mocellin, M. Abbate, B. G. Searle, P. T. Fonseca, and E. Morikawa, *Phys. Rev. B* **77**, 075118 (2008).

- ¹⁹J. Mendialdua, R. Casanova, and Y. Barbaux, *J. Electron Spectrosc. Relat. Phenom.* **71**, 249 (1995).
- ²⁰G. Silversmit, D. Depla, H. Poelman, G. B. Marin, and R. De Gryse, *J. Electron Spectrosc. Relat. Phenom.* **135**, 167 (2004).
- ²¹M. J. van Setten, S. Er, G. Brocks, R. A. de Groot, and G. A. de Wijs, *Phys. Rev. B* **79**, 125117 (2009).
- ²²D. G. Ouellette, S. Lee, J. Son, S. Stemmer, L. Balents, A. J. Millis, and S. J. Allen, *Phys. Rev. B* **82**, 165112 (2010).
- ²³D. N. Basov, R. D. Averitt, D. van der Marel, M. Dressel, and K. Haule, *Rev. Mod. Phys.* **83**, 471 (2011).
- ²⁴L. Zhang, Y. Zhou, L. Guo, W. Zhao, A. Barnes, H.-T. Zhang, C. Eaton, Y. Zheng, M. Brahlek, H. F. Haneef, N. J. Podraza, M. H. W. Chan, V. Gopalan, K. M. Rabe, and R. Engel-Herbert, *Nat. Mater.* **15**, 204 (2016).
- ²⁵A. Zylbersztein and N. F. Mott, *Phys. Rev. B* **11**, 4383 (1975).
- ²⁶M. W. Haverkort, Z. Hu, A. Tanaka, W. Reichelt, S. V. Streltsov, M. A. Korotin, V. I. Anisimov, H. H. Hsieh, H.-J. Lin, C. T. Chen, D. I. Khomskii, and L. H. Tjeng, *Phys. Rev. Lett.* **95**, 196404 (2005).
- ²⁷E. Arcangeletti, L. Baldassarre, D. Di Castro, S. Lupi, L. Malavasi, C. Marini, A. Perucchi, and P. Postorino, *Phys. Rev. Lett.* **98**, 196406 (2007).
- ²⁸M. M. Qazilbash, A. A. Schafgans, K. S. Burch, S. J. Yun, B. G. Chae, B. J. Kim, H. T. Kim, and D. N. Basov, *Phys. Rev. B* **77**, 115121 (2008).
- ²⁹T. Yao, X. Zhang, Z. Sun, S. Liu, Y. Huang, Y. Xie, C. Wu, X. Yuan, W. Zhang, Z. Wu, G. Pan, F. Hu, L. Wu, Q. Liu, and S. Wei, *Phys. Rev. Lett.* **105**, 226405 (2010).
- ³⁰N. B. Aetukuri, A. X. Gray, M. Drouard, M. Cossale, L. Gao, A. H. Reid, R. Kukreja, H. Ohldag, C. A. Jenkins, E. Arenholz, K. P. Roche, H. A. Dürr, M. G. Samant, and S. S. P. Parkin, *Nat. Phys.* **9**, 661 (2013).
- ³¹S. Kumar, J. P. Strachan, M. D. Pickett, A. Bratkovsky, Y. Nishi, and R. S. Williams, *Adv. Mater.* **26**, 7505 (2014).
- ³²S. Lee, T. L. Meyer, C. Sohn, D. Lee, J. Nichols, D. Lee, S. S. A. Seo, J. W. Freeland, T. W. Noh, and H. N. Lee, *APL Mater.* **3**, 126109 (2015).
- ³³S. Choi, S.-J. Chang, J. Oh, J. H. Jang, and S. Lee, *Adv. Electron. Mater.* **4**, 1700620 (2018).